Breast Cancer Detection by Optomechanical Imaging

Rabah Al abdi[1], Harry L. Graber[1,2], Yong Xu[1,2], and Randall L. Barbour[1,2]
[1]SUNY Downstate Medical Center,450 Clarkson Ave, Brooklyn NY 11203
[2]NIRx Medical Technologies LLC, 15 Cherry Lane, Glen Head NY 11545, USA

Abstract:
A new functional imaging system, which combines precise mechanical articulation and dynamic optical tomography for the detection breast cancer, is presented. Results obtained indicate that a wealth of new contrast features is accessible.

Introduction:
The character of the information obtained using different sensing methods can be additive or wholly new, depending on whether the different sensing domains interact or not. In an attempt to exploit elements of the tumor phenotype involving increased stiffness [1], and enhanced angiogenesis [2], recently we have developed the method of optomechanical imaging as a new approach for the detection of breast cancer [3].

By combining precise articulation of the breast with concurrent optical measures, it is feasible to explore the viscoelastic and hemodynamic properties of the breast as a function of a wide range of protocols that serve to effectively enhance tumor contrast.

Here we outline the principal elements of system functionality and present representative clinical finding documenting that a wealth of new contrast features is accessible.

Instrumentation:
The developed imaging system supports three distinct classes of measures:
- ✓ Optical data using high-density optode arrangements (32 sources and 64 detectors).
- ✓ Applied force using 16 semiconductor strain gauges.
- ✓ Breast shape and tissue deformation during mechanical provocations.

Fig. 1 shows schematics and a photograph of the developed optomechanical system.

Mechanical measures are achieved using a feedback-controlled articulation assembly that can effect measures of creep and stress relaxation. Individual control of each articulating element supports a wide array of applied force maneuvers involving full, partial, wave-like or vibratory compression protocols.

Fig. 2 is a functional diagram of the imager. A TTL signal generated from the optical switch controller (inset 3) is used to encode the position of the optical switch, control the gain level in the detection boards, and synchronize the operation of the system controller (1) and the articulating sensing head controller (2).

Fig. 3 is a close-up view of one of the sensing heads used for simultaneous bilateral studies attached to the balloon phantom (Fig 3a), and to the torso phantom (Fig 3b).

Table 1 summarizes the principal performance features of the articulating breast imager. Principal features include the ability to acquire concurrent optical and mechanical measures simultaneously from both breasts with high signal fidelity. Additionally, bilateral measures can be made without mechanical interference, and the system can accommodate a wide range of breast sizes (B–DD cup sizes) with the subject in the seated position.

Methods:
Because image reconstruction makes use of a fixed-size finite element model, while the experimental study encompasses a large range of breast sizes as well as mechanical manipulating and deformation, measurements were carried out with the balloon phantom to evaluate and quantify the effects of changing the boundary conditions. In these experiments, an electrochromic cell (ECC) inside the balloon phantom was driven with a 0.1-Hz square wave. Fig 4 shows the 0.1-Hz component of the normalized power spectral density computed from the reconstructed image time series of the 830-nm absorption coefficient.

The mechanical provocation protocol involves full compression, medio-lateral (ML) relaxation, cranio-caudal (CC) relaxation, ML compression, and ML relaxation. This sequence is carried out at two different force amplitudes (4.4 and 7.1 N). In each case, the target force was reached within a few seconds and finger positions were held fixed for one minute. Table 2 reports measures of positional error and temporal fidelity of the recovered image of the ECC, as a function of the provocation protocol.

By applying mechanical compression and decompression to modulate the hemodynamics of the breast, six classes of optical response occur simultaneously. Some of them are purely hemodynamic responses, while others are dominated by the changes in optical pathlength between the source-detector pairs (Fig 4).

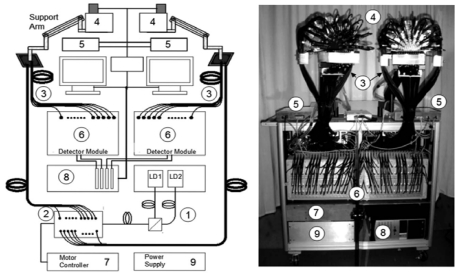

Fig. 1: Developed dual-breast articulating imager. (a) Schematic and (b) photograph of imager: laser sources and coupling optics (1), two-stage optical switch (2), illumination and detection fiber optics (3), sensor heads and support arms (4), stepper motor drivers (5), detector modules (6), servo-motor controller (7), host computer (8), and system power supply (9). LD = laser diode.

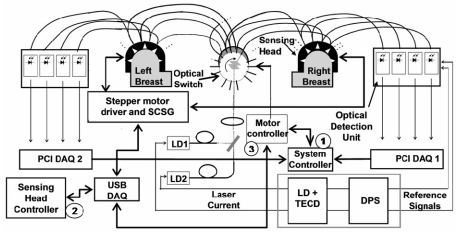

Fig. 2: Schematic of the overall system architecture of the breast imager. (LD) Laser diode, (TECD) Thermo electric cooler driver, (DPS) Digital Phase Shifter, (SGSC) Strain gauge semiconductor.

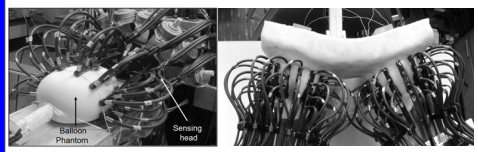

Fig. 3: Photographs showing the sensing heads and calibrating breast phantoms (static and dynamic).

Table 2: Positional error and temporal fidelity of recovered ECC image

Condition	μ_{a760} $(x\text{-}x_0, y\text{-}y_0, z\text{-}z_0)$	ρ	μ_{a830} $(x\text{-}x0, y\text{-}y0, z\text{-}z0)$	ρ
Baseline	(0, 3, -3)	0.97	(0, 1, -3)	0.99
Full comp.	(0, 0, -3)	0.94	(0, -.1, -3)	0.96
ML relax.	(-1, 0, -3)	0.95	(-1, -2, -3)	0.95
CC relax.	(0, 0, -3)	0.94	(-1, -1, -3)	0.98
ML comp.	(1, 0, -4)	0.92	(2, -2, -5)	0.97

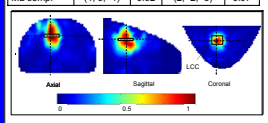

Fig 4 Axial, sagittal, and coronal cross-sections of the 3D normalized PSD, at 0.1 Hz, of the 830 nm absorption coefficient.

Table 1: Optical and mechanical specifications of the breast imager

PARAMETER	VALUE
Wavelengths	760 and 830 nm
Number of sources	64 (32 left and 32 right)
Number of detectors	128 (64 left and 64 right)
Detector sensitivity	10 pW
Dynamic range	1:109 (180 dB)
Cross talk (optical)	< 1: 10^{-5}
Cross talk (electronic)	< 1:10^{-6}
Data acquisition rate	1.8 Hz x 8192 channels
Force sensitivity	0.04 N (0.01 lb)
Capacity	15 N (3.4 lb)
Cross talk	1 : 10^{-3}
Repeatability (STD)	0.08 N (0.02 lb)
SR movement range	90 mm
Data acquisition rate	20 Hz x 16 channels

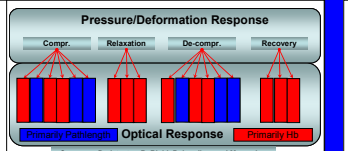

Fig. 4: Schematic of different classes of optical responses during mechanical provocation.

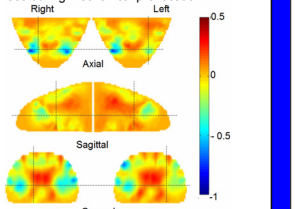

Fig. 5. 3D image of Hb_{Tot} response to applied force, for a 38 y/o healthy subject.

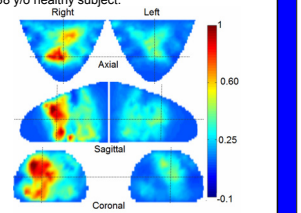

Fig. 6. 3D image of Hb_{Tot} response to applied force, for a 40 y/o cancer patient with a 6 cm intraductal carcinoma in the right breast .

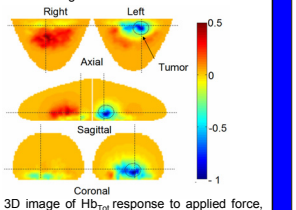

Fig. 7: 3D image of Hb_{Tot} response to applied force, for a 50 y/o patient with a 4 cm invasive ductal carcinoma in the left breast. (backreflection measurement)

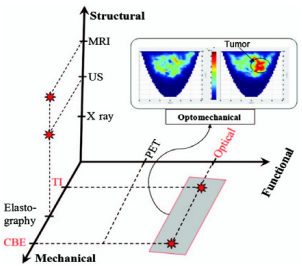

Fig. 8: Sensing domains for breast cancer detection.

Results:
The quantity plotted in Fig. 5 is a linear combination of temporal means of total hemoglobin (HbTot) images corresponding to four different 1 min time intervals: the 60 s periods immediately preceding and following the 4.2 N ML unloading, and also the 60 s periods immediately preceding and following the 7.1 N ML unloading. Then we computed the difference between the temporal-mean images for the first and second of the four 60 s intervals and likewise of the third and fourth intervals Finally, the first difference was subtracted from the second difference, in order to evaluate the pressure dependence of the HbTot response. Images were reconstructed from transmission channels only (S-R D-M and S-M D-R, Fig. 4), and they were normalized to their maximum absolute values. The subject was 38 y/o with a BMI of 33 and size D breasts. Inspection reveals:
- A larger decrease in Hb_{Tot} in the medial and lateral portions of the breast.
- An increase in Hb_{Tot} in the central region.
- Similar hemodynamic responses in both breasts.

Shown in Fig. 6 are the results of a similar difference-image computation, for a cancer patient who was 40 y/o with a BMI of 37 and a 6 cm intraductal carcinoma in the right breast (a minor difference from the preceding case is that here the 4.4 N and 7.1 N forces were applied by all of the articulating elements). A diffuse area of increased contrast, which coincides with the known tumor location, is evident in the right breast. Notably, the unaffected (left) breast shows a diffuse response with substantially reduced contrast in comparison to the right breast.

Shown in Fig. 7 is a spatial map of contrast features revealed by computing the average slope of the HbTot response, normalized to its maximum absolute value, seen during the 60 s stress-relaxation period immediately following the 5.4N full compression (i.e., force was applied by all eight articulating units). Images were reconstructed from backreflection channels only (S-R D-R, non-moving, lower sensing array). The participant was 50 years old, with a BMI of 44 and a 4 cm invasive ductal carcinoma in the left breast. Contrary to the unaffected breast, the tumor-bearing breast reveals a negative slope, indicating that HbTot levels continue to decline throughout the period of stress relaxation.

Summary:
Imaging studies of the breast comprise three principal sensing domains: structural, functional and mechanical. Combinations of these can yield either additive or wholly new information, depending on whether one domain interacts with the other. As summarized in Fig. 4, by implementing tactile sensing with precisely controlled articulation (similar to elements of the CBE), combined with high-density optical measures, we have implemented a new imaging technique that can explore a wide range of functional responses that are sensitive to viscoelastic and hemodynamic disturbances that are known to be associated with breast tumors.

Future studies will focus on the optimization of the protocols and use of sufficiently stable and accurate modeling techniques.

References:
[1] S. Kumar and V. M. Weaver, “Mechanics, malignancy, and metastasis:the force journey of a tumor cell,” Cancer Metastasis Rev. **28**, 113–127 (2009).
[2] P. Vaupel, F. Kallinowski, and P. Okunieff, “Blood flow, oxygen and nutrient supply, and metabolic microenvironment of human tumors: a review,” Cancer Res. **49**, 6449–6465 (1989).
[3] R. Al abdi, H.L. Graber, Y. Xu, and R.L. Barbour, “Optomechanical imaging system for breast cancer detection,” *J. Optical Society of America* A, **28**, 2473-2493 (2011).

Acknowledgements:
This research was supported by the National Institutes of Health (NIH) grant R41CA096102, the U.S. Army grant DAMD017-03-C-0018, the Susan G. Komen Foundation, the New York State Department of Health (Empire Clinical Research Investigator Program), the New York State Foundation for Science, Technology and Innovation–Technology Transfer Incentive Program (NYSTAR-TIPP) grant C020041, and NIRx Medical Technologies.